PAPER

Cation dynamics by ^1H and ^{13}C MAS NMR in hybrid organic–inorganic $(CH_3CH_2NH_3)_2CuCl_4$

Ae Ran Lim [ID] *[ab] and Yong Lak Joo [ID] [c]

To understand the dynamics of the cation in layered perovskite-type $(CH_3CH_2NH_3)_2CuCl_4$, the temperature-dependent chemical shifts and spin–lattice relaxation times $T_{1\rho}$ in the rotating frame have been measured using ^1H magic angle spinning nuclear magnetic resonance (MAS NMR) and ^{13}C cross-polarization (CP)/MAS NMR techniques. Each proton and carbon in the $(CH_3CH_2NH_3)^+$ cation is distinguished in MAS NMR spectra. The Bloembergen–Purcell–Pound (BPP) curves for ^1H $T_{1\rho}$ in CH_3CH_2 and NH_3, and for the ^{13}C $T_{1\rho}$ in CH_3 and CH_2 are revealed to have minima at low temperatures. This implies that the curves represent the CH_3 and NH_3^+ rotational motions. The amplitude of the cationic motion is enhanced at the C-end, that is, the N-end of the organic cation is fixed to the inorganic layer through N–H···Cl hydrogen bonds, and $T_{1\rho}$ becomes short with larger-amplitude molecular motions.

I. Introduction

Metal–organic hybrids, which consist of organic and inorganic components, have recently attracted much attention because these materials have many possibilities for the tailoring of their functionalities and physical properties including optical, electrical and magnetic properties by adjusting the organic and/or metal building blocks. Hybrid metal–organic compounds based on the perovskite structures are of increasing interest due to their potential use for solar cells.[1,2] However, toxicity and chemical instability issues of halide perovskites still remain as the main drawbacks for use in solar cells. The crystalline structure of compounds of the type $(C_nH_{2n+1}NH_3)_2MCl_4$, where n = 1, 2, 3 … and M represents divalent metals (M = Cu, Cd, …), may be described as a sequence of alternating organic–inorganic layers.[3–6] Many compounds in this family have been extensively investigated and have demonstrated successive phase transitions. This family of materials crystallizes in the layered perovskite structure, which consists of infinite, staggered layers of corner-sharing MCl_6 octahedra interleaved by alkylammonium cations.[7] Because of the layered character of their structure, these crystals become appropriate substances for investigations of two-dimensional electronic systems. The cavities between the octahedra are occupied by the ammonium heads of the organic cations, which, importantly, form strong N–H···Cl hydrogen bonds to any of the eight chloride ions.[8]

^{a}*Analytical Laboratory of Advanced Ferroelectric Crystals, Jeonju University, Jeonju 55069, South Korea. E-mail: aeranlim@hanmail.net; arlim@jj.ac.kr; Tel: +82-63-220-2514*

^{b}*Department of Science Education, Jeonju University, Jeonju 55069, South Korea*

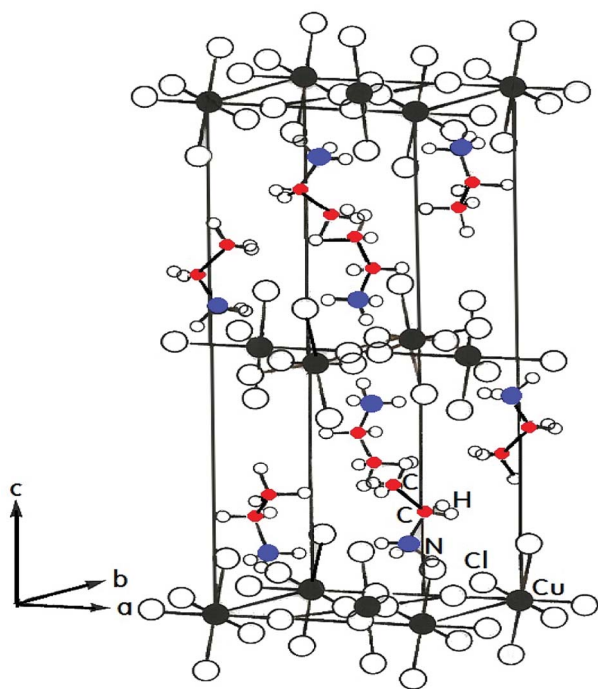^{c}*School of Chemical and Biomolecular Engineering, Cornell University, Ithaca, New York 14853, USA*

Ethylammonium copper chloride $(CH_3CH_2NH_3)_2CuCl_4$ is a layered perovskite-type compound that undergoes a complicated sequence of phase transitions. Differential scanning calorimetry (DSC) data indicates several phase transitions, at 236 K ($=T_{C4}$), 330 K ($=T_{C3}$), 357 K ($=T_{C2}$), and 371 K ($=T_{C1}$), as temperature increases.[9–14] The peaks at 236 K, 330 K, and 371 K are very weak and can perhaps correspond to second-order transformations.[13] The phase transitions in this crystal are mostly connected with changes in the arrangement of the alkylammonium chains. Fig. 1 shows the room-temperature orthorhombic crystal structure of $(CH_3CH_2NH_3)_2CuCl_4$.[8,15] The hybrids have the orthorhombic crystal structure with the space group *Pbca*, and the lattice constants are a = 7.47 Å, b = 7.35 Å, and c = 21.18 Å at room temperature.[16] The $CuCl_6$ octahedra are strongly distorted with elongated Cu–Cl bonds orthogonal to each other on adjacent octahedra. The $CuCl_6$ sheets are sandwiched between two layers of alkylammonium. The structure of the organic component consists of a double layer of alkylammonium ions with their charged ends, the nitrogen atoms, oriented to the nearest $CuCl_6$ plane.[4] The complete structure is constituted by corner-sharing $CuCl_6$ octahedra, forming the inorganic layers, and bilayers of organic cations attached to the octahedra by their NH_3 heads.[17,18]

The structural geometry and molecular motions of the organic molecules within the layered hybrid structure is important for determining the influence of temperature on the evolution of the structural phase transitions in the perovskite structure. Physical properties in particular depend on the characteristics of metallic anion and the organic cation.

In the present study, the crystal structure and thermal stability for $(CH_3CH_2NH_3)_2CuCl_4$ was observed by means of conventional X-ray, thermogravimetric analysis (TGA), and optical polarizing microscopy. In order to clarify the structural geometry and

Fig. 1 Orthorhombic structure of a $(CH_3CH_2NH_3)_2CuCl_4$ crystal at room temperature.

dynamics of the cation in the organic–inorganic $(CH_3CH_2NH_3)_2$-$CuCl_4$, we investigated the chemical shifts and the spin–lattice relaxation time $T_{1\rho}$ in the rotating frame using ^1H magic angle spinning nuclear magnetic resonance (MAS NMR) and ^{13}C cross-polarization (CP)/MAS NMR. The CH_3CH_2 and NH_4 groups of the $CH_3CH_2NH_3$ cation are distinguishable in ^1H MAS NMR spectra, and the CH_3 and CH_2 groups are distinguished by ^{13}C CP/MAS NMR spectra. We investigated the ^1H and ^{13}C dynamics in the $(CH_3CH_2NH_3)^+$ cation near the phase-transition temperatures.

II. Experimental method

Crystals of $(CH_3CH_2NH_3)_2CuCl_4$ were obtained by slow evaporation at 25 °C from an aqueous solution of $C_2H_5NH_2\cdot HCl$ and $CuCl_2\cdot 2H_2O$ in the stoichiometric 2 : 1 proportion. The obtained crystals were yellow square plates, typically 5 mm × 5 mm in area and 0.5 mm in thickness.

The structure of the $(CH_3CH_2NH_3)_2CuCl_4$ crystals was determined at room temperature with an X-ray diffraction system (PANalytical, X'pert pro MPD) with a Cu-Kα ($\lambda = 1.5418$) radiation source. Measurements were taken in a θ–2θ geometry from 10° to 60° at 45 kV and with a tube power of 40 mA. And, the TGA curve at a heating rate of 10 °C min^{-1} was measured under N_2 atmosphere, and the mass of the powdered sample used in the TGA experiment was 11.41 mg.

The chemical shifts and the $T_{1\rho}$ values for $(CH_3CH_2NH_3)_2$-$CuCl_4$ were obtained by ^1H MAS NMR and ^{13}C CP/MAS NMR at Larmor frequencies of $\omega_0/2\pi = 400.13$ and 100.61 MHz, respectively, using Bruker 400 MHz NMR spectrometers at the Korea Basic Science Institute, Western Seoul Center. Crystalline powdered samples were placed within a 4 mm CP/MAS probe,

and the MAS rate for ^1H and ^{13}C measurements, to minimize spinning sideband overlap, was set to 10 kHz. The ^1H $T_{1\rho}$ values were determined using a $\pi/2-t$ sequence by varying the duration of spin-locking pulses. ^{13}C $T_{1\rho}$ values were measured by varying the duration of the spin-locking pulse applied after the CP preparation period. The width of the $\pi/2$ pulse used for measuring $T_{1\rho}$ for ^1H and ^{13}C was 3.7 μs, with the spin-locking field at 67.56 kHz. The chemical shifts and $T_{1\rho}$ were measured over a temperature range of 180–430 K.

III. Experimental results

The measured structure at room temperature exhibited orthorhombic symmetry with cell parameters of $a = 7.480$ Å, $b = 7.375$ Å, $c = 21.254$ Å for $(CH_3CH_2NH_3)_2CuCl_4$ crystal. This result is consistent with the results reported by Steadman and Willett.[16]

The TGA curve of $(CH_3CH_2NH_3)_2CuCl_4$ is shown in Fig. 2 for measuring thermal stability. The first occurrence of mass loss begins at approximately 430 K (T_d), which is the onset of partial thermal decomposition. The second weight loss of 25.1% near 530 K is due to the removal of the $CH_3CH_2NH_3Cl$ from the compound, leaving intermediate $CH_3CH_2NH_3CuCl_3$ that belongs to another known class of compounds ABX_3. Near 560 K, $CuCl_2$ remains as the residue and when it reaches 580 K, the total weight loss becomes 65.55%. The color of the crystal is dark yellow at room temperature although it has slightly inhomogeneous hue due to surface roughness. As the temperature increases, the color of the crystal varies from dark yellow (300 K, 350 K), brown (400 K), to dark brown (450 K, 500 K), and then they start melting at 530 K as shown in the inset in Fig. 2. The TGA and optical polarizing microscopy results show that the crystal above 430 K allows CH_3 to partially escape by the breaking the weak C–N bond.

The ^1H NMR spectra at a frequency of 400.13 MHz were obtained by MAS NMR. The ^1H spectrum recorded at room
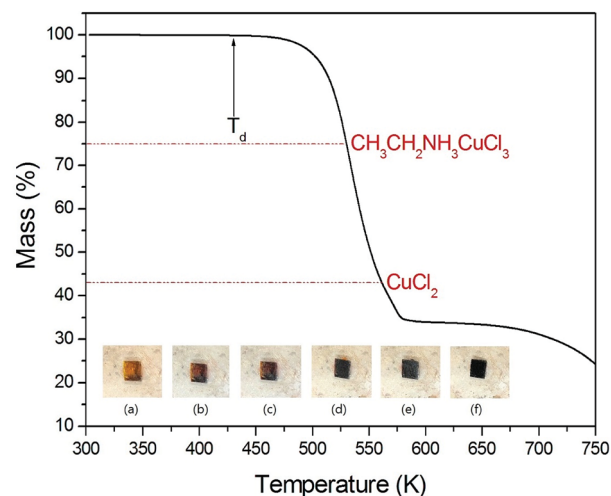

Fig. 2 Thermogravimetric analysis of $(CH_3CH_2NH_3)_2CuCl_4$ (inset: color changes of a $(CH_3CH_2NH_3)_2CuCl_4$ crystal according to the temperature): (a) 300 K, (b) 350 K, (c) 400 K, (d) 450 K, (e) 500 K, and (f) 530 K.

temperature is shown in the inset in Fig. 3; the spectrum shows two peaks at chemical shifts of $\delta = 0.23$ and 12.12 ppm, which are assigned to the protons of the CH_3CH_2 and NH_3 groups, respectively. The spinning sidebands for CH_3CH_2 are marked with asterisks and those for NH_3 are marked with open circles. However, the different ^1H signals from CH_3 and CH_2 cannot be resolved, and therefore the combined CH_3CH_2 peak is very broad and has a larger intensity due to the overlap of the CH_3 and CH_2 peaks. The peak with the lower chemical shift is attributed to the protons in CH_3CH_2, and that of the higher chemical shift is attributed to the protons in NH_3. The ^1H chemical shifts for the alkyl and ammonium groups slowly and monotonously vary with temperature, indicating that the surrounding environments of the protons in the alkyl and ammonium groups change continuously, as shown in Fig. 3; here, the chemical shifts for protons in CH_3CH_2 and NH_3 near T_{C1}, T_{C2}, and T_{C3} are nearly constant with temperature, whereas those for protons in CH_3CH_2 and NH_3 below T_{C4} change more abruptly.

The $T_{1\rho}$ values for the CH_3CH_2 and NH_3 protons in $(CH_3CH_2NH_3)_2CuCl_4$ were obtained as a function of temperature. The magnetization traces of both the alkyl and ammonium protons may be described by a single exponential function[19–21]

$$S(t)/S_0 = \exp(-t/T_{1\rho}), \qquad (1)$$

where $S(t)$ is the magnetization as a function of the spin-locking pulse duration t, and S_0 is the total nuclear magnetization of the proton at thermal equilibrium.[19] The recovery curves for several delay times were measured, and the $T_{1\rho}$ values were obtained from the slopes by the delay time vs. intensity, at several different temperatures. This analysis method was used to obtain the $T_{1\rho}$ values for each proton in CH_3CH_2 and NH_3 which are plotted as a function of inverse temperature in Fig. 4. The $T_{1\rho}$ values for the CH_3CH_2 and NH_3 protons in the $(CH_3CH_2NH_3)^+$ cations exhibit similar trends with temperature. The
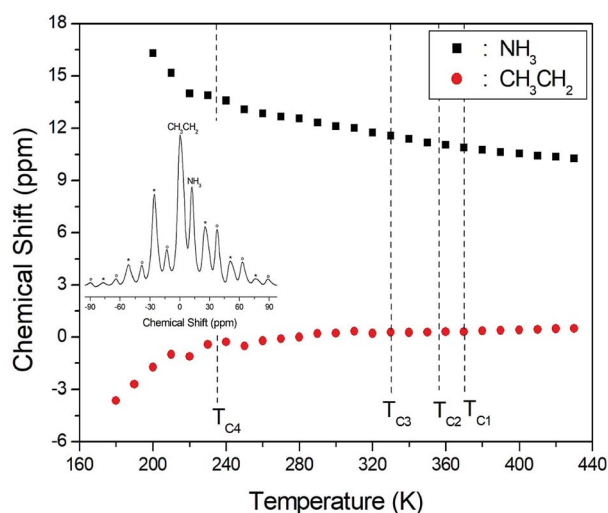
proton $T_{1\rho}$ data do not show evidence of a change near the phase-transition temperature; the $T_{1\rho}$ values of protons in the CH_3CH_2 and NH_3 groups of $(CH_3CH_2NH_3)_2CuCl_4$ are almost continuous near T_{C1}, T_{C2}, and T_{C3}, and these values are of the order of few milliseconds. The $T_{1\rho}$ values abruptly decreased with temperature in the region approaching T_{C4}. The relaxation time for the ^1H nucleus is minimal at 190 K and 200 K for CH_3CH_2 and NH_3, respectively. This feature of $T_{1\rho}$ indicates that distinct molecular motions are present. The $T_{1\rho}$ values are related to the corresponding values of the rotational correlation time, τ_C, which is a direct measure of the rate of molecular motion. For the spin–lattice relaxation time in the rotating frame, the experimental value of $T_{1\rho}$ can be expressed in terms of the correlation time τ_C for the molecular motion, as suggested by the Bloembergen–Purcell–Pound (BPP) function:[19,22]

$$T_{1\rho}^{-1} = (N/20)(\gamma_H\gamma_C\hbar/r_{H-C}{}^3)^2\{4\tau_C/(1 + \omega_1{}^2\tau_C{}^2)$$
$$+ \tau_C/[1 + (\omega_H - \omega_C)^2\tau_C{}^2] + 3\tau_C/[1 + (\omega_C{}^2\tau_C{}^2)]$$
$$+ 6\tau_C/[1 + (\omega_H + \omega_C)^2\tau_C{}^2] + 6\tau_C/[1 + \omega_H{}^2\tau_C{}^2]\}. \qquad (2)$$

Here, γ_H and γ_C are the gyromagnetic ratios for the ^1H and ^{13}C nuclei, respectively; N is the number of directly bound protons; r_{H-C} is the H–C internuclear distance; $\hbar$ is the reduced Planck constant; ω_H and ω_C are the Larmor frequencies of ^1H and ^{13}C, respectively; and ω_1 is the frequency of the spin-locking field. We analyzed our data assuming that $T_{1\rho}$ would show a minimum when $\omega_1\tau_C = 1$, and that the BPP relation between $T_{1\rho}$ and the characteristic frequency ω_1 could be applied. We sensitively controlled the minima in the $T_{1\rho}$ temperature variations and the slopes around the minima. From these results, the value of $(\gamma_H\gamma_C\hbar/r_{H-C}{}^3)^2$ for the proton in eqn (2) was obtained. We then calculated the temperature dependences of the τ_C values for protons by using the obtained values of $(\gamma_H\gamma_C\hbar/r_{H-C}{}^3)^2$. The temperature dependence of τ_C follows a simple Arrhenius equation:
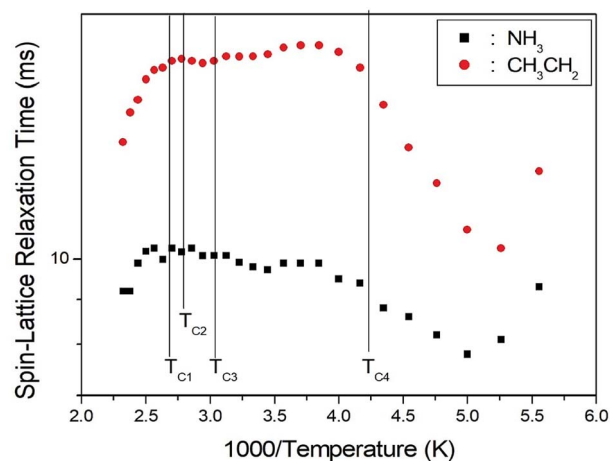
$$\tau_C = \tau_0 \exp(-E_a/RT), \qquad (3)$$

Fig. 3 Chemical shifts for ^1H MAS NMR of $(CH_3CH_2NH_3)_2CuCl_4$ as a function of temperature (inset: ^1H MAS NMR spectrum of $(CH_3CH_2NH_3)_2CuCl_4$ at 300 K with spinning sidebands indicated by asterisks and open circles).

Fig. 4 ^1H spin–lattice relaxation times $T_{1\rho}$ in the rotating frame for the CH_3CH_2 and NH_3 groups of $(CH_3CH_2NH_3)_2CuCl_4$ as a function of inverse temperature.

where τ_0 is a pre-exponential factor, T is the temperature, R is the gas constant, and E_a is the activation energy. Thus, the slope of the linear portion of a semi-log plot should yield E_a. The E_a value for the rotational motion can be obtained from the log τ_C *vs.* $1000/T$ curve shown in Fig. 5; we obtained $E_a = 12.19 \pm 1.30$ kJ mol^{-1} and $E_a = 8.33 \pm 0.50$ kJ mol^{-1} for CH$_3$CH$_2$ and NH$_3$, respectively. The rotational motion for alkyl groups is activated, whereas the rotational motion for ammonium groups at the end of the organic cation is less strongly activated.

The structural analysis of the carbons in (CH$_3$CH$_2$NH$_3$)$_2$CuCl$_4$ was performed by ^{13}C CP/MAS NMR, and the corresponding spectrum is shown in Fig. 6, as a function of temperature; the ^{13}C CP/MAS NMR spectrum at room temperature shows two signals at chemical shifts of $\delta = 50.77$ ppm and $\delta = 113.50$ ppm with respect to tetramethysilane (TMS), which can be assigned to CH$_3$ and CH$_2$, respectively. The ^{13}C chemical shift of CH$_2$ abruptly shifts with temperature, whereas that of CH$_3$ changes only much
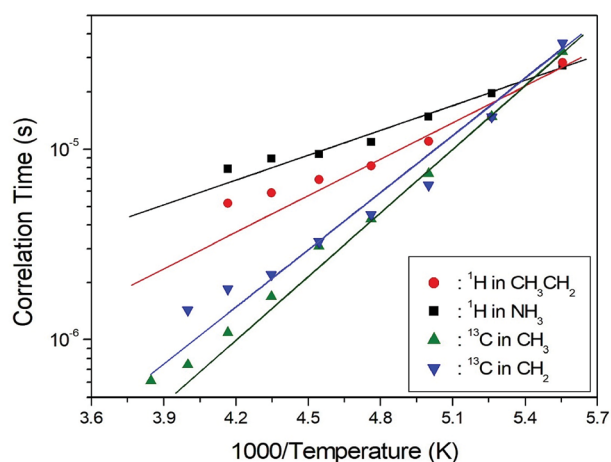

Fig. 7 Temperature dependences of line widths of ^{13}C NMR spectra of CH$_3$ and CH$_2$ in (CH$_3$CH$_2$NH$_3$)$_2$CuCl$_4$.

less with temperature. The full width at half maximum (FWHM) linewidths for the ^{13}C of CH$_3$ and CH$_2$ in Fig. 7 showed a monotonic decrease with increasing temperature, with no particular anomalies attributable to the phase transitions. The linewidth of the ^{13}C signal assigned to CH$_3$ is broad compared to that of CH$_2$, and the linewidth narrows significantly with increasing temperature. This narrowing of the ^{13}C linewidths is attributed to internal motions that the line widths follow the same temperature dependence as some internal motions, hence the motions are responsible for the line widths.

To obtain the ^{13}C $T_{1\rho}$ values, the nuclear magnetization was also measured at several temperatures as a function of delay time. The signal intensity of the nuclear magnetization recovery curves for ^{13}C is described by a single exponential function as in eqn (1) at all temperatures. The ^{13}C $T_{1\rho}$ values for CH$_3$ and CH$_2$ in (CH$_3$CH$_2$NH$_3$)$_2$CuCl$_4$ are plotted as a function of inverse temperature in Fig. 8. The temperature dependences of the ^{13}C MAS NMR $T_{1\rho}$ values seem to be similar. The $T_{1\rho}$ values for CH$_3$ and CH$_2$ both

Fig. 5 Arrhenius plots of the natural logarithm of the correlation time for each ^{1}H and ^{13}C of (CH$_3$CH$_2$NH$_3$)$_2$CuCl$_4$ as a function of inverse temperature.
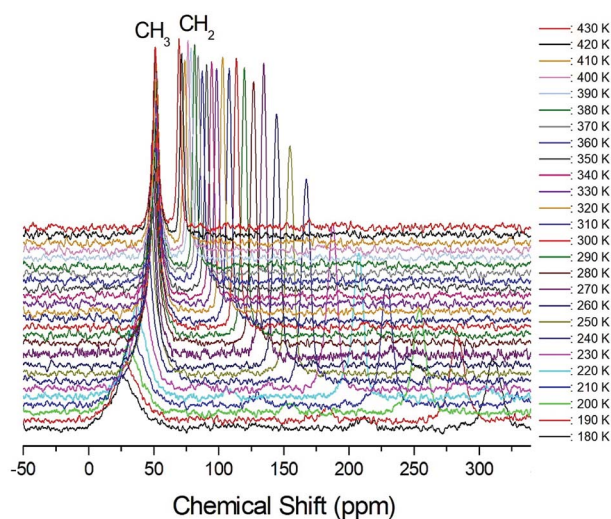

Fig. 6 ^{13}C CP/MAS NMR spectra of (CH$_3$CH$_2$NH$_3$)$_2$CuCl$_4$ measured at different temperatures.

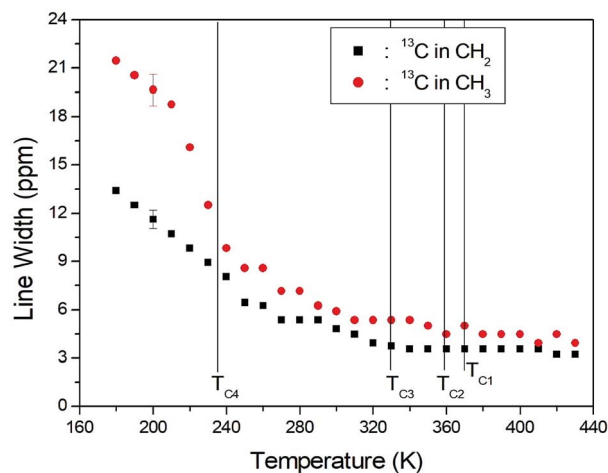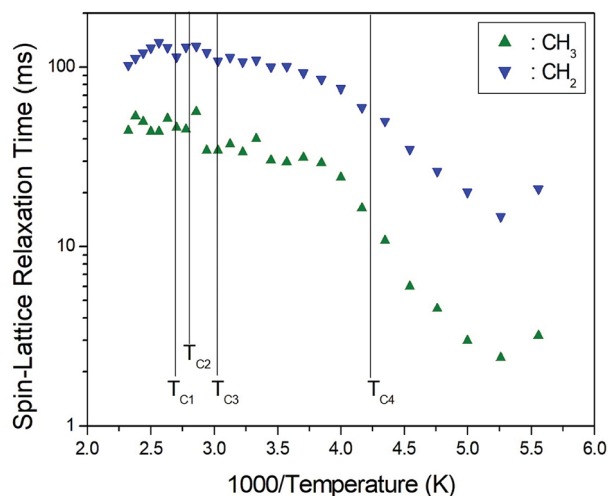Fig. 8 ^{13}C spin−lattice relaxation times $T_{1\rho}$ in the rotating frame for CH$_3$ and CH$_2$ in (CH$_3$CH$_2$NH$_3$)$_2$CuCl$_4$ as a function of inverse temperature.

increase with temperature in the same manner; whereas, the ^{13}C $T_{1\rho}$ values near the phase-transition temperatures are approximately continuous. The $T_{1\rho}$ values for CH_3 and CH_2 at room temperature are 33.85 ms and 109.40 ms, respectively. The amplitude of the cationic motion is enhanced at its CH_3 end, and the central CH_2 moiety is fixed to the NH_3 group in the organic cation. The $T_{1\rho}$ curve below T_{C4} can be reproduced by BPP theory. The BPP curves for CH_3 and CH_2, showing minima at low temperatures, is almost the same as those of the CH_3CH_2 and NH_3 shifts of the ^{1}H MAS NMR measurements. E_a for the rotational motion of CH_3 and CH_2 can be obtained from the log τ_C vs. $1000/T$ curve shown in Fig. 5; we obtained $E_a = 21.35 \pm 0.45$ kJ mol^{-1} for CH_3 and $E_a = 19.72 \pm 1.76$ kJ mol^{-1} for CH_2, respectively, which, considering their error ranges, are the same values.

IV.   Conclusion

We discuss the molecular motions for cation of Cu-based hybrid materials, where we replace Pb with nontoxic Cu metal for lead-free perovskite solar cells, and investigate their potential toward solar cell applications based on ionic dynamics of the cation in hybrid organic–inorganic $(CH_3CH_2NH_3)_2CuCl_4$ by NMR studies. The cation dynamics and interionic interactions through hydrogen bonds are expected to be closely related with the physical properties due to the potential applications. The cation dynamics in a layered perovskite-type $(CH_3CH_2NH_3)_2CuCl_4$ were investigated as a function of temperature by ^{1}H MAS NMR and ^{13}C CP/MAS NMR experiments. The CH_3CH_2 and NH_4 units in the $CH_3CH_2NH_3$ cation were distinguished by the ^{1}H MAS NMR spectra, and the CH_3 and CH_2 units in the $CH_3CH_2NH_3$ cation were also clearly distinguished in the ^{13}C CP/MAS NMR spectra. To obtain detailed information about the cation dynamics of this crystal, the spin–lattice relaxation time $T_{1\rho}$ in the rotating frame for both ^{1}H and ^{13}C were measured, revealing that these atoms undergo rotational motions at low temperatures. The BPP curves for the ^{1}H $T_{1\rho}$ in CH_3CH_2 and NH_3, and for the ^{13}C $T_{1\rho}$ in CH_3 and CH_2, were shown to have a minimum at low temperatures; the $T_{1\rho}$ of ^{1}H and ^{13}C showed a minimum and is governed by the tumbling motion of the CH_3CH_2 and NH_3 groups, indicating that the ^{1}H and ^{13}C atoms in the CH_3CH_2-NH_3^+ groups exhibit high mobility at low temperatures. The molecular motions for ^{1}H and ^{13}C in the $CH_3CH_2NH_3^+$ cation were very free at low temperatures. $T_{1\rho}$ provides insight into the changes in the cation reorientation rates at low temperature.

The ^{13}C $T_{1\rho}$ values in CH_3 increased with temperature, a trend that has been observed in alkyl chains attached to the $(CH_3$-$CH_2NH_3)$ cation due to its greater mobility toward its free end. The $CH_3CH_2NH_3$ cationic motion is enhanced at the opposing end of the cation to the NH_4^+ group probably because this group is bound to the inorganic layer through the N–H⋯Cl hydrogen bonds. The ^{13}C $T_{1\rho}$ is usually dominated by the fluctuation of the anisotropic chemical shift, and it becomes shorter with larger-amplitude molecular motions. This implies that the amplitude of the cationic motion is enhanced at the C-end, that is, the N-end of the organic cation is fixed at the inorganic layer through N–H⋯Cl hydrogen bonds. The cationic motion, being associated with the fluctuation of the molecular axis, is expected to be gradually excited with increasing temperature.

Conflicts of interest

There are no conflicts to declare.

Acknowledgements

References

1 A. M. Elseman, A. E. Shalan, S. Sajid, M. M. Rashad, A. M. Hassan and M. Li, *ACS Appl. Mater. Interfaces*, 2018, **10**, 11699.

2 J. A. Aramburu, P. Garcia-Fernandez, N. R. Mathiesen, J. M. Garcia-Lastra and M. Moreno, *J. Phys. Chem. C*, 2018, **122**, 5071.

3 A. Caretta, M. C. Donker, A. O. Polyakov, T. T. M. Palstra and P. H. M. van Loosdrecht, *Phys. Rev. B: Condens. Matter Mater. Phys.*, 2015, **91**, 20405.

4 E. Suprayoga, A. A. Nugroho, A. O. Polyakov, T. T. M. Palstra and I. Watanabe, *J. Phys.: Conf. Ser.*, 2014, **551**, 12054.

5 J. Ding, H. Li, L. Wen, X. Kang, H. Li and J. Zhang, *J. Magn. Magn. Mater.*, 2013, **346**, 91.

6 R. Lefi, F. B. Naser and H. Guermazi, *J. Alloys Compd.*, 2017, **696**, 1244.

7 K. Ohwada, K. Ishii, T. Inami, Y. Murakami, T. Shobu, H. Ohsumi, N. Ikeda and Y. Ohishi, *Phys. Rev. B: Condens. Matter Mater. Phys.*, 2005, **72**, 14123.

8 B. Kundys, A. Lappas, M. Viret, V. Kapustianyk, V. Rudyk, S. Semak, Ch. Simon and I. Bakaimi, *Phys. Rev. B: Condens. Matter Mater. Phys.*, 2010, **81**, 224434.

9 V. Kapustianyk, V. Rudyk and M. Partyka, *Phys. Status Solidi B*, 2007, **244**, 2151.

10 V. B. Kapustianik, V. V. Bazhan and Yu. M. Korchak, *Phys. Status Solidi B*, 2002, **234**, 674.

11 W. Kleemann, F. J. Schafer, E. Karajamaki, R. Laiho and T. Levola, *Physica B*, 1983, **119**, 269.

12 V. Kapustianik, Yu. Korchak, I. Polovinko, R. Tchukvinskyi, Z. Czapla and S. Dacko, *Phys. Status Solidi B*, 1998, **207**, 95.

13 C. B. Mohamed, K. Karoui, F. Jomni, K. Guidara and A. B. Rhaiem, *J. Mol. Struct.*, 2015, **1082**, 38.

14 I. R. Jahn, K. Knorr and J. Ihringer, *J. Phys.: Condens. Matter*, 1989, **1**, 6005.

15 P. Zolfaghari, G. A. de Wijs and R. A. de Groot, *J. Phys.: Condens. Matter*, 2013, **25**, 295502.

16 J. P. Steadman and R. D. Willett, *Inorg. Chim. Acta*, 1970, **4**, 367.

17 A. O. Polyakov, A. H. Arkenbout, J. Baas, G. R. Blake, A. Meetsma, A. Caretta, P. H. M. van Loosdrecht and T. T. M. Palstra, *Chem. Mater.*, 2012, **24**, 133.

18 A. Caretta, R. Miranti, R. W. A. Havenith, E. Rampi, M. C. Donker, G. R. Blake, M. Montagnese, A. O. Polyakov, R. Broer, T. T. M. Palstra and P. H. M. van Loosdrecht, *Phys. Rev. B: Condens. Matter Mater. Phys.*, 2014, **89**, 24301.

19 J. L. Koenig, *Spectroscopy of Polymers*, Elsevier, New York, 1999.

20 V. J. Mcbrierty and K. J. Packer, *Nuclear Magnetic Resonance in Solid Polymers*, Cambridge University Press, Cambridge, 1993.

21 A. R. Lim, *RSC Adv.*, 2018, **8**, 18656.

22 A. R. Lim, *RSC Adv.*, 2017, **7**, 55276.